Arch. Met. Geoph. Biocl., Ser. A 34, 3–26 (1985)

ARCHIVES
FOR METEOROLOGY,
GEOPHYSICS, AND
BIOCLIMATOLOGY

551.553.1

[1] Department of Atmospheric Science, Colorado State University, Fort Collins, Colorado, U.S.A., and
[2] Institut für Physik, GKSS-Forschungszentrum, Geesthacht, Federal Republic of Germany

A Numerical Study of the Effects of a Large Sandbar upon Sea Breeze Development

R. C. Kessler[1], D. Eppel[2], R. A. Pielke[1], and J. McQueen[1]

With 7 Figures

Received November 27, 1984

Summary

Two-dimensional numerical simulations of sea breeze development over a large sandbar on the North Sea coast of Germany are reported. The numerical model used in these experiments contains a detailed treatment of soil moisture, which allows evaluation of the effects of differential surface characteristics on the airflow pattern. Results of the simulations indicate that the contrast between the moist sandbar and adjacent dry land, the tidal inundation of the sandbar, and the westward penetration of the Baltic sea breeze play important roles in the development of mesoscale airflow patterns in the sandbar region.

Zusammenfassung

Eine numerische Studie des Einflusses einer großen Sandbank auf die Entwicklung der Seebrise

Die zweidimensionale, numerische Simulierung der Seebrisenentwicklung über einer großen Sandbank an der Nordseeküste Deutschlands wird beschrieben. Das hier angewandte Modell enthält eine detaillierte Behandlung der Bodenfeuchte, welche eine Auswertung des Effektes differenzierter Oberflächencharakteristika auf die Luftströmung erlaubt. Rechnungsresultate zeigen, daß der Kontrast zwischen Sandbank und benachbartem, trockenem Land, die gezeitenbewirkte Überflutung der Sandbank und die nach Osten vorrückende Seebrise der Ostsee eine wichtige Rolle in der Entwicklung von mesoskalaren Strömungsverteilungen im Gebiet der Sandbank spielen.

1. Introduction

Along the North Sea coast of Germany there exist extensive areas of sand which are inundated at high tide, and which are above water at low tide.

These sandbars are depicted by the shaded areas shown on the map in Fig. 1.

As these sandbars extend up to fifteen to twenty kilometers out into the sea, their inundation might be expected to exert a major effect on the local airflow in this area. Sea-breeze circulations are generated by land-water surface temperature contrasts. Tidal inundation (or recession) produces a significant horizontal displacement of the zone of maximum surface temperature contrast, to which the atmosphere must respond. Though the transition is strongly dependent on the local topography of the sandbars the inundation takes place on a time scale of one hour.

When the sandbar is above water, the difference in surface heating between the moist sand and the drier soil at adjacent inland locations is expected to also affect the local airflow pattern.

To our knowledge, the effects of sandbars on atmospheric airflows have not heretofore been studied[1]. In this introductory study, we utilize two-dimensional mesoscale numerical simulations to assess the response of the atmosphere to a large sandbar of uniform composition. However, we are aware that the morphology of this coastal region [11] is more complex. The resulting parameterization of friction and moisture flux is therefore only approximate.

The numerical model utilized in this study is a two-dimensional form of a primitive-equation, hydrostatic incompressible model originally developed by Pielke [9] for the study of sea breezes in south Florida. The model includes a surface heat budget [10] and a treatment of soil moisture effects [5]. This model appears to be well suited to the study of airflows generated by differential surface heating.

2. Model Description

The basic equations for the numerical model are given in Mahrer and Pielke [3], along with a detailed description of the treatments of the atmospheric surface layer, planetary boundary layer, and radiative fluxes. The fluxes of momentum, heat, and moisture in the atmospheric surface layer are parameterized according to Businger [1]. The height of the planetary boundary layer is determined from a prognostic equation proposed by Deardorff [2]. Turbulent exchange coefficients are computed according to the method of O'Brien [6], based on the surface layer fluxes and the planetary boundary layer (PBL) height.

At land locations a surface heat balance equation is solved iteratively for surface temperature in each grid column as described by Mahrer and

[1] The influence of wet ground juxtaposed against dry ground, however, has been sumulated for several selected cases (e.g. see [7]).

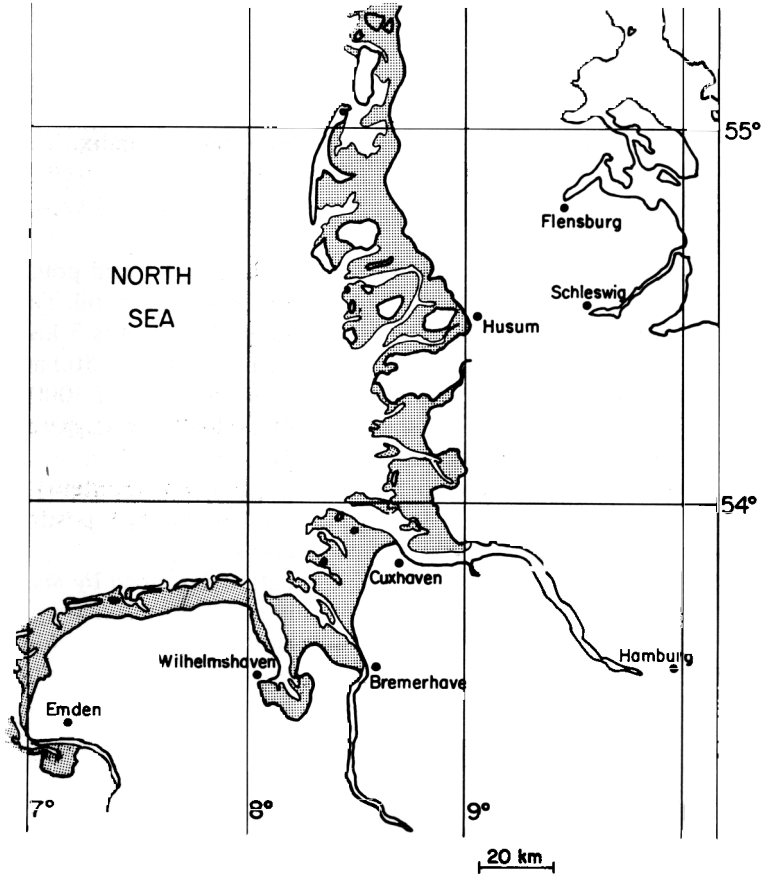

Fig. 1. The North Sea coast of Germany. The sandbar areas are shaded

Pielke [3]. This equation imposes a balance among (1) the net fluxes of short and long-wave radiation; (2) the turbulent atmospheric fluxes of sensible and latent heat above the air-soil interface; and (3) the flux of heat into the soil below the interface. A one-dimensional diffusion equation is solved at each land grid point for soil temperature.

The treatment of the moisture fluxes at the air-soil interface is discussed in detail by McCumber and Pielke [5]. We predict the soil moisture content through a specified depth of the soil, and impose continuity of the moisture flux at the air-soil interface through an iterative process.

Since the flux of latent heat is directly proportional to the flux of water vapor, the soil moisture characteristics effectively govern the partition of incoming solar radiation between sensible and latent heating in this model.

Characteristic soil parameters for the textural classes assigned in this study are given in Table A1. It is well known that the flux characteristics of the ground may change considerably when a plant canopy is present. However, the synoptic situation we have considered is coincident with the period shortly after harvest time where large portions of the ground are bare soil.

At the ground, a no-slip condition is imposed on velocity. On water surfaces, θ is held constant at 292 K; the air immediately above a water surface is assumed to be saturated. At the land points, θ_s and η are held constant at a depth of 50 cm.

We assume a roughness length of 0.1 cm for the sandbar, and 4 cm for all other soils.

At the lateral boundaries of the model domain, zero-gradient boundary conditions are imposed on u, v, θ, and q. The upper boundary is a material surface whose height is predicted as described by Mahrer and Pielke [3]; on this surface, u, v, θ, and q remain constant.

5. Initial Conditions

The initial conditions assigned for these simulations are representative of a summertime synoptic pattern which results in maximum daytime land-water temperature contrasts along the coasts of Schleswig-Holstein. This pattern is dominated by a stagnant high pressure ridge centered over northern Scandinavia. The easterly flow at low levels associated with this pattern produces abnormally hot and dry daytime conditions over much of Germany, with maximum temperatures at inland surface stations frequently in excess of 30 °C.

The model is initialized at local sunrise, computed for 1 August at latitude 55 N (0415 LST). The initial atmospheric profiles of θ and q are assumed to be horizontally homogeneous; these are given in Table 2.

Table 2. *Initial Profiles of θ and q*

z (m)	θ (K)	q (g kg^{-1})	z (m)	θ (K)	q (g kg^{-1})
5000	307.25	0.5	1250	296.0	4.5
4750	306.5	0.5	750	294.5	5.5
4350	305.0	0.5	350	293.5	6.5
3750	303.5	0.5	150	292.6	7.9
3250	302.0	1.0	75	292.0	8.1
2750	300.5	1.5	37.5	291.0	8.3
2250	299.0	2.5	17.5	290.0	8.5
1750	297.5	3.5	6	289.0	8.7

Table 3. *Initial Soil θ Profile*

Depth (cm)	θ (K)	Depth (cm)	θ (K)
0	288.0	5	289.0
1	288.2	7.5	290.3
2	288.4	20	291.0
3	288.6	30	291.0
4	288.8	50	289.5

Table 4. *Initial Values of Soil Moisture Content*

Soil type	Clay loam	Loam	Loamy sand	Sand (dry)	Sand (wet)
η	0.19	0.135	0.06	0.06	0.24

A uniform synoptic-scale geostrophic wind of 4 ms^{-1} from 90 degrees is assumed throughout the model domain. The height of the planetary boundary layer is initially assumed to be 200 m; within the PBL an Ekman-balanced initial wind profile is computed.

The initialization of the soil variables is rather arbitrary, as there is little observational guidance. θ_s is initially assumed to be horizontally homogeneous, with the initial vertical profile given in Table 3. McCumber and Pielke [5] report that their model results are relatively insensitive to variations in the initial soil temperature profile.

At each land grid point the soil moisture content η is initially assumed constant with depth. The initial value of η assigned to each soil region is given in Table 4. For the sandbar region, we assign an initial value of η sufficient to maintain air saturation at the air-soil interface throughout a 12-hour one-dimensional simulation initialized as described above. Over the remaining soil regions it is assumed that significant drying of the soil has taken place before the time of initialization. Beinhauer (personal communication) estimates soil moisture contents of 15–30% of field capacity in northern Schleswig-Holstein after several hot summer days without rain. Initial values of η assumed for dry sand and sandy loam in our experiments are approximately equal to 0.15 η_s. However, in preliminary tests we were unable to obtain convergence of the atmospheric and soil moisture fluxes at clay loam and loam surfaces with η initially set at 0.15 η_s. Thus, η was initially set at 0.40 η_s for clay loam and 0.30 η_s for loam; these are the lowest values which allowed convergence of the moisture fluxes throughout a 12-hour simulation.

6. Treatment of the Tidal Cycle

Based on the observed behavior of the sandbars off the west coast of Schleswig-Holstein, we approximate the tidal cycle by the following idealization: we assume that "high tide" persists for 4 hours, while "low tide" persists for 8 hours.
The tidal transition is assumed to take place over a 30-minute period. In grid boxes within the sandbar region, the fraction of the grid box assumed to be covered by sand decreases linearly from 1 to 0 over this period; similarly, the water fraction increases linearly from 0 to 1. During the period of inundation, two profiles of the turbulent exchange coefficients for heat and momentum are computed for each grid column over the sandbar. One profile is based on the surface characteristics of the sand, obtained via the surface heat and moisture budgets. The other profile is computed assuming a water surface of constant temperature. Resultant K profiles are then obtained by weighting the land- and water-based K profiles according to the land-water distribution within the grid box at the given time.

7. Sensitivity of the Model to Soil Variability

To isolate and compare the response of the model atmosphere to the soil surfaces specified in this study, we carried out a series of one-dimensional column simulations similar to those reported by McCumber and Pielke [5]. Since advective effects are absent in these simulations, all variability among the simulation results is ascribable to differences in the response of the soil surface to incoming solar energy. The initial conditions for each simulation are identical to those specified as initial conditions for an individual column with the given soil type in the two-dimensional simulations. The integration time is 12 hours and the time step is 30 s, as in the two-dimensional simulations.
We summarize the relevant results of these simulations in Table 5. Here

Table 5. *Results of One-Dimensional Simulations*

Soil type	$\Delta\theta$ (K)		Min. Relative Humidity (%)		Max. Bowen Ratio
	Surface	$z = 6$ m	Surface	$z = 6$ m	
Clay loam	27.7	12.8	13	22	9.1
Loam	21.5	10.7	28	32	1.4
Loamy sand	25.3	12.0	15	24	6.4
Sand (dry)	22.6	11.1	23	29	2.2
Sand (wet)	10.2	6.6	100	67	0.14

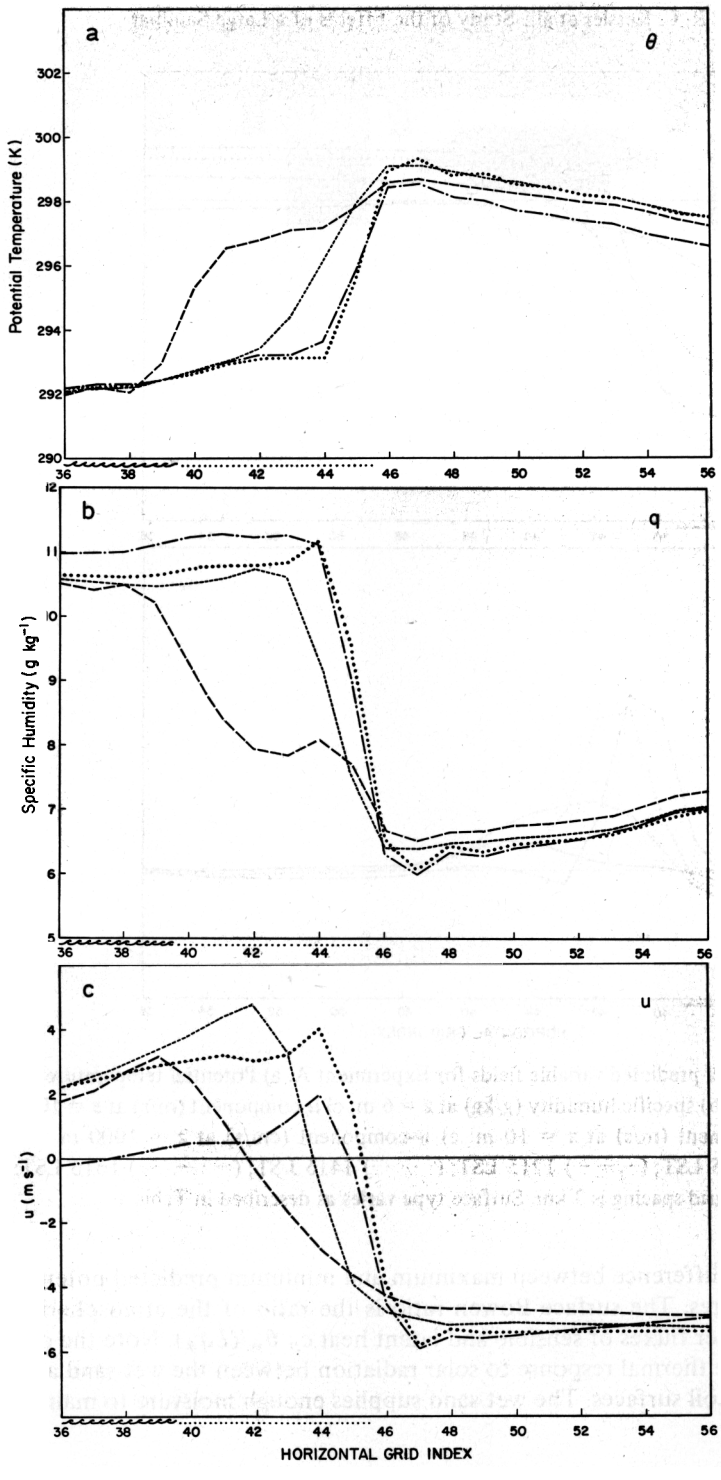
a
θ
Potential Temperature (K)
302
300
298
296
294
292
290
36
38
40
42
44
46
48
50
52
54
56
b
q
Specific Humidity (g kg⁻¹)
12
11
10
9
8
7
6
5
c
u
u (m s⁻¹)
4
2
0
-2
-4
-6
HORIZONTAL GRID INDEX

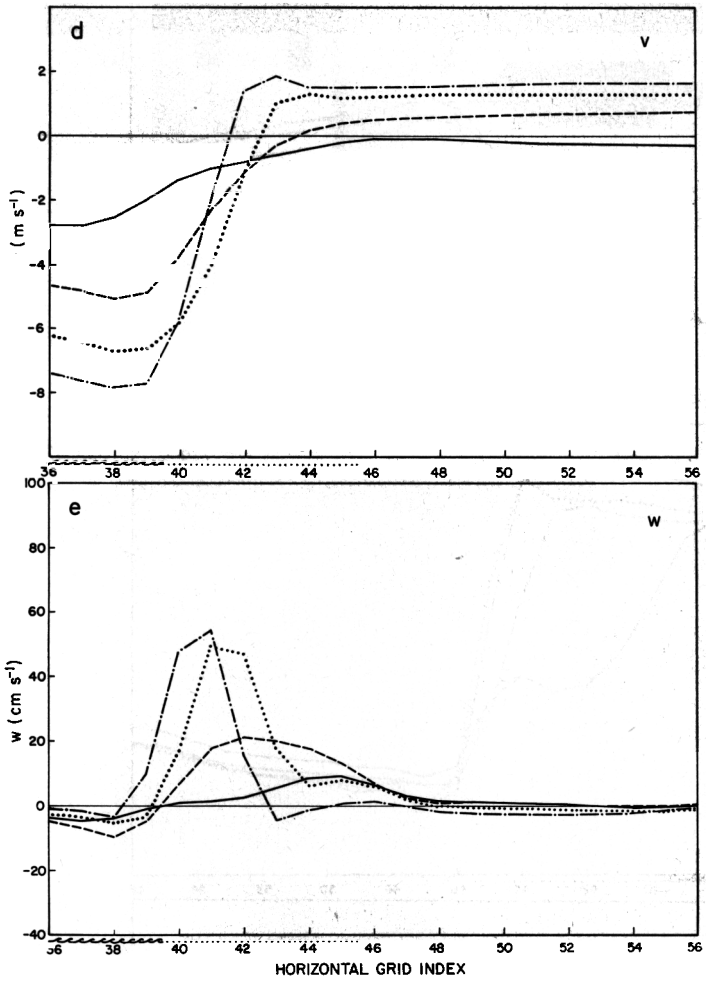

Fig. 2. Model-predicted variable fields for Experiment A. a) Potential temperature (K) at $z = 6$ m; b) specific humidity (g/kg) at $z = 6$ m; c) u-component (m/s) at $z = 10$ m; d) v-component (m/s) at $z = 10$ m; e) w-component (cm/s) at $z = 1000$ m. (——) 1015 LST; (— — —) 1215 LST; (· · · · ·) 1415 LST; (— · — · —) 1615 LST. Horizontal grid spacing is 3 km. Surface type varies as described in Table 1

$\Delta\theta$ is the difference between maximum and minimum predicted potential temperatures. The surface Bowen ratio is the ratio of the atmospheric surface layer fluxes of sensible and latent heat $c_p\ \theta_*/(Lq_*)$. Note the difference in the thermal response to solar radiation between the wet sand and the other soil surfaces. The wet sand supplies enough moisture to maintain

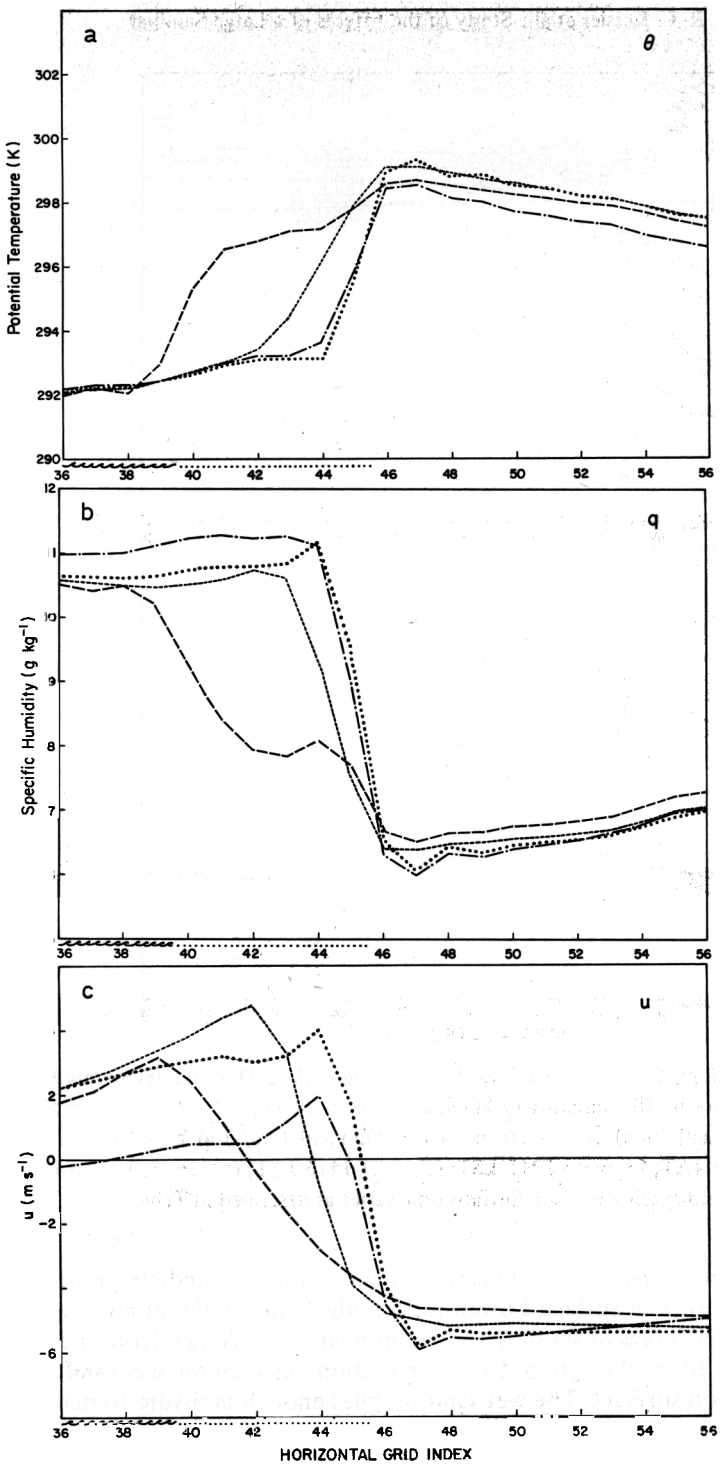
a
θ
Potential Temperature (K)
302
300
298
296
294
292
290
36
38
40
42
44
46
48
50
52
54
56
b
q
Specific Humidity (g kg⁻¹)
12
11
10
9
8
7
c
u
u (m s⁻¹)
2
0
-2
-6
HORIZONTAL GRID INDEX

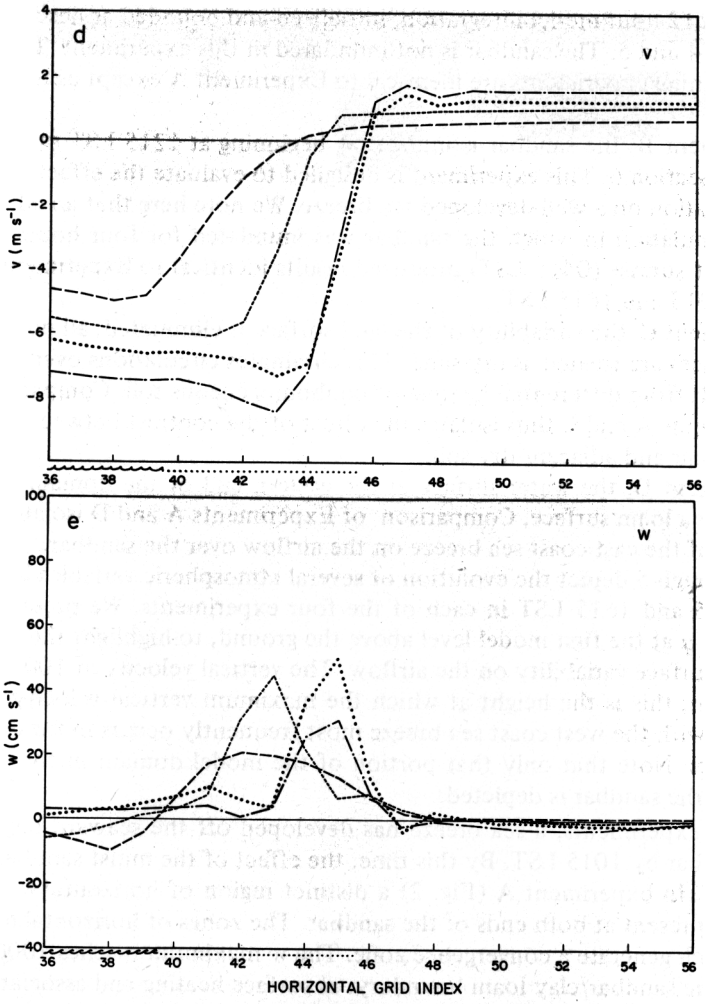

Fig. 3. Same as Fig. 2, for Experiment B, except (— — —) 1215 LST; (- - -) 1315 LST; (· · · · ·) 1415 LST; (— · — · —) 1615 LST

saturation at the air-soil interface. Thus, more of the incoming solar energy is channeled into evaporation than into sensible heating. As indicated by the surface relative humidities, the remaining soils dry out significantly as they are heated by the sun.

8. Sea-Breeze Simulations

In this section we consider the daytime airflow pattern in the vicinity of the sandbar. Four two-dimensional numerical simulations are discussed. Experi-

ment A is a 12-hour model integration, initialized and bounded as described in Sections 4 and 5. The sandbar is not inundated in this experiment. The three remaining experiments are identical to Experiment A except as noted below.

In Experiment B, the sandbar is inundated beginning at 1215 LST as described in Section 6. This experiment is designed to evaluate the effect of tidal inundation on a well-developed sea breeze. We note here that an additional simulation in which the sandbar was inundated for four hours beginning at sunrise (0415 LST) produced results identical to Experiment A between 1015 and 1615 LST.

In Experiment C, the variability of the land surface is eliminated; all non-water surfaces are treated as dry sand. This eliminates circulations over land which result from differential heating of nonhomogeneous soil. Comparison of experiments A and C thus isolates the effect of the contrast between the moist sandbar and adjacent dry soil.

In Experiment D, the water surface at the eastern end of the domain is replaced by a loam surface. Comparison of Experiments A and D isolates the effect of the east coast sea breeze on the airflow over the sandbar.

Figs. 2 through 5 depict the evolution of several atmospheric variables between 1015 and 1615 LST in each of the four experiments. We present u, v, θ, and q at the first model level above the ground, to highlight the effects of surface variability on the airflow. The vertical velocity at 1000 m is also given; this is the height at which the maximum vertical velocity associated with the west coast sea breeze most frequently occurs in these experiments. Note that only that portion of the model domain in the vicinity of the sandbar is depicted.

In all four experiments, a sea breeze has developed off the seaward edge of the sandbar by 1015 LST. By this time, the effect of the moist sandbar is apparent. In experiment A (Fig. 2) a distinct region of horizontal θ gradient is present at both ends of the sandbar. The zones of horizontal θ gradient each generate a convergence zone. The w maximum reaches 1000 m first near the sandbar/clay loam boundary, as surface heating and associated boundary layer growth are more rapid at this location than at the seaward edge of the sandbar. In Experiment C (Fig. 4), where the moist sandbar and clay loam are replaced by dry sand, a sharp surface θ gradient occurs only at the sea/land boundary, with an associated w maximum at 1000 m.

The surface characteristics and the east coast sea breeze (ESB) each exert a significant effect on the predicted movement of the west coast sea breeze (WSB) after 1015 LST. Because $\partial\theta/\partial x$ is positive above the entire extent of the sandbar in Experiment A, the WSB moves further eastward between 1015 and 1215 LST than it does in Experiment C, where $\partial\theta/\partial x$ east of the WSB front is virtually zero. The w maximum in Experiment A shifts westward during this period as the boundary layer grows near the west coast.

The effect of the ESB becomes significant during the afternoon. The ESB is diffuse, with no significant associated convergence zone. In Experiment A the penetration of the ESB erodes the horizontal θ gradient above the east edge of the sandbar; as a result, the WSB front is pushed back toward the west coast. However, in Experiment D (Fig. 5), in which the ESB is absent, the WSB front moves continuously eastward between 1015 and 1615 LST.

The results of Experiment B (Fig. 3) illustrate the adjustment of the WSB to tidal inundation. After inundation is complete (1245 LST) a significant surface temperature discontinuity exists only at the boundary between the inundated sandbar and the relatively hot clay loam surface. The WSB front moves past this boundary approximately 1 hour after the completion of inundation. This indicates the time required for the atmospheric boundary layer to respond to the inundated surface. As in Experiment A, westward movement of the WSB front appears after 1415 LST; the westward movement is substantially less in Experiment B than in Experiment A because the ESB does not significantly erode the horizontal θ gradient.

A significant northerly wind component is associated with the WSB in each of the experiments. The development of the WSB results in an inertial imbalance which feeds into the v component via the term $-f(u-u_g)$. Note that in Experiment B the inertial imbalance persists after inundation removes the sea/sandbar interface; thus the northerly flow continues to intensify over the inundated sandbar, while the westerly component weakens significantly between 1415 and 1615 LST.

The surface heat budget for the non-water surfaces in Experiment A is given for 1215 and 1615 LST in Fig. 6. Over the dry soil (i.e. non-sand bar), the magnitude of each term in the surface heat budget is nearly constant within each soil region. The atmospheric response to the differential heating of the various dry soils is smoothed by advection (Fig. 2a).

The differences in surface response between the moist sandbar and the dry soils are quite significant. The sandbar receives a greater net radiative influx than do the dry soils, primarily as a result of its lower surface albedo as determined by (A17). As indicated by the one-dimensional experiments of the previous section, the latent heat flux dominates the sensible heat flux over the sandbar, while the reverse is true over the dry soils.

Note that the heat flux into the moist sand at 1215 LST is much greater than the heat flux into the dry soils despite the cooler sandbar surface. The magnitude of this flux is ascribable to the high thermal conductivity of moist sand (eq. A16).

In Fig. 7 we show the behavior of the specific humidity at the ground surface, q_0, in the vicinity of the sandbar in Experiment A. A pronounced q_0 maximum occurs on the sandbar, due to the combined effects of sensible heating (which increases the saturation specific humidity at the surface), and upward transfer of moisture within the sand (which maintains surface

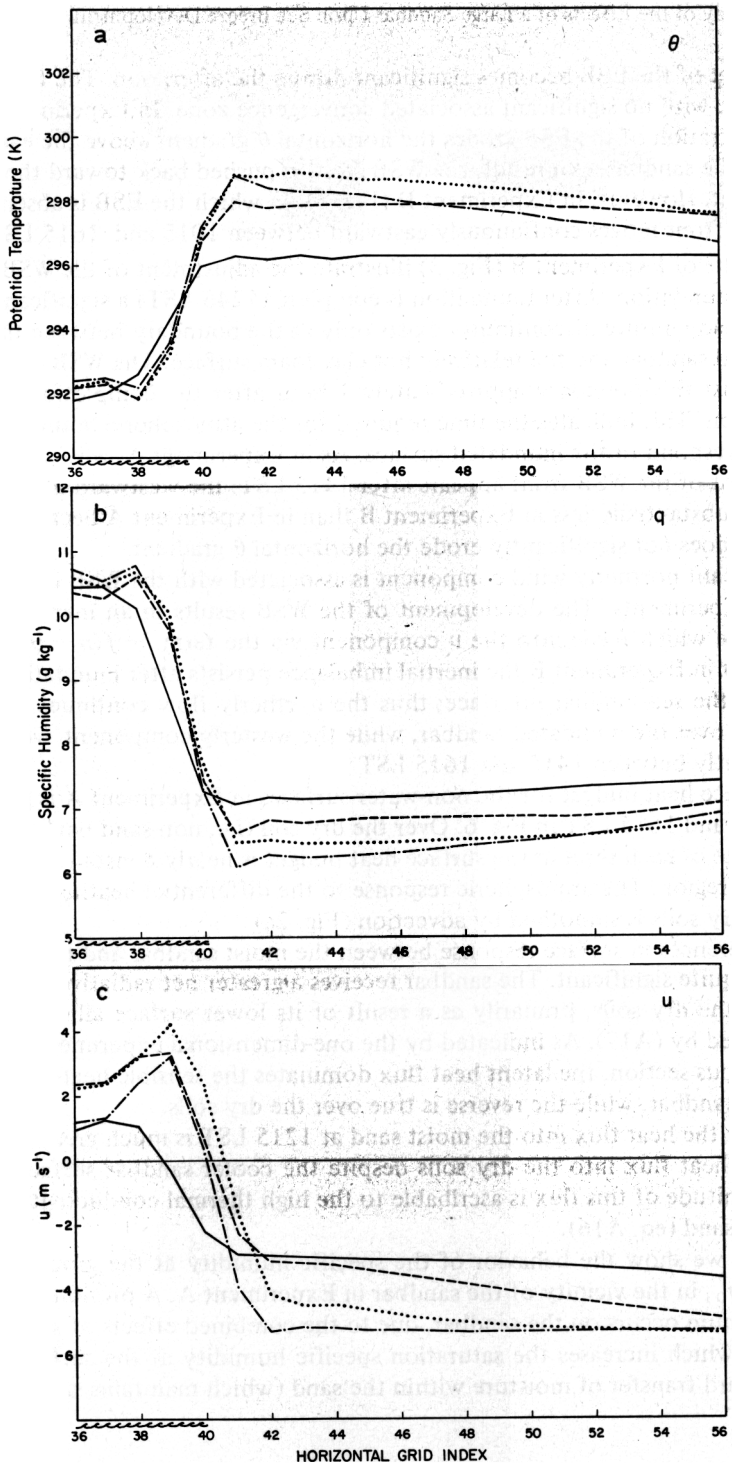
a
θ
Potential Temperature (K)
302
300
298
296
294
292
290
36
38
40
42
44
46
48
50
52
54
56
b
q
Specific Humidity (g kg⁻¹)
12
11
10
9
8
7
6
5
c
u
u (m s⁻¹)
4
2
0
-2
-4
-6
HORIZONTAL GRID INDEX

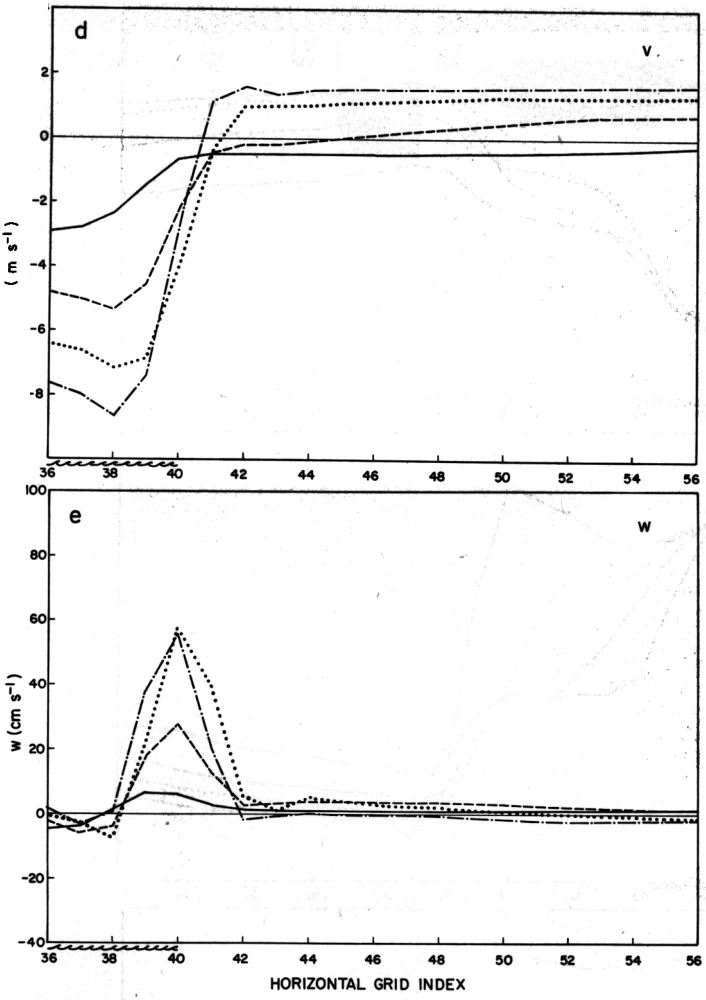

Fig. 4. Same as Fig. 2, for Experiment C

saturation). However, 6 m above the sandbar surface (Fig. 2b) q decreases during the first 6 h of model integration as advection from the dry soil region dominates the turbulent transfer of moisture from below (Fig. 2a). After passage of the WSB front, q levels above the sandbar rise as marine air is advected eastward.

Between 1415 and 1615 LST, q increases sharply at the 6 m level in Experiment A above the eastern portion of the sandbar. Since this region lies east of the WSB front, drier air is advected into the region from inland.

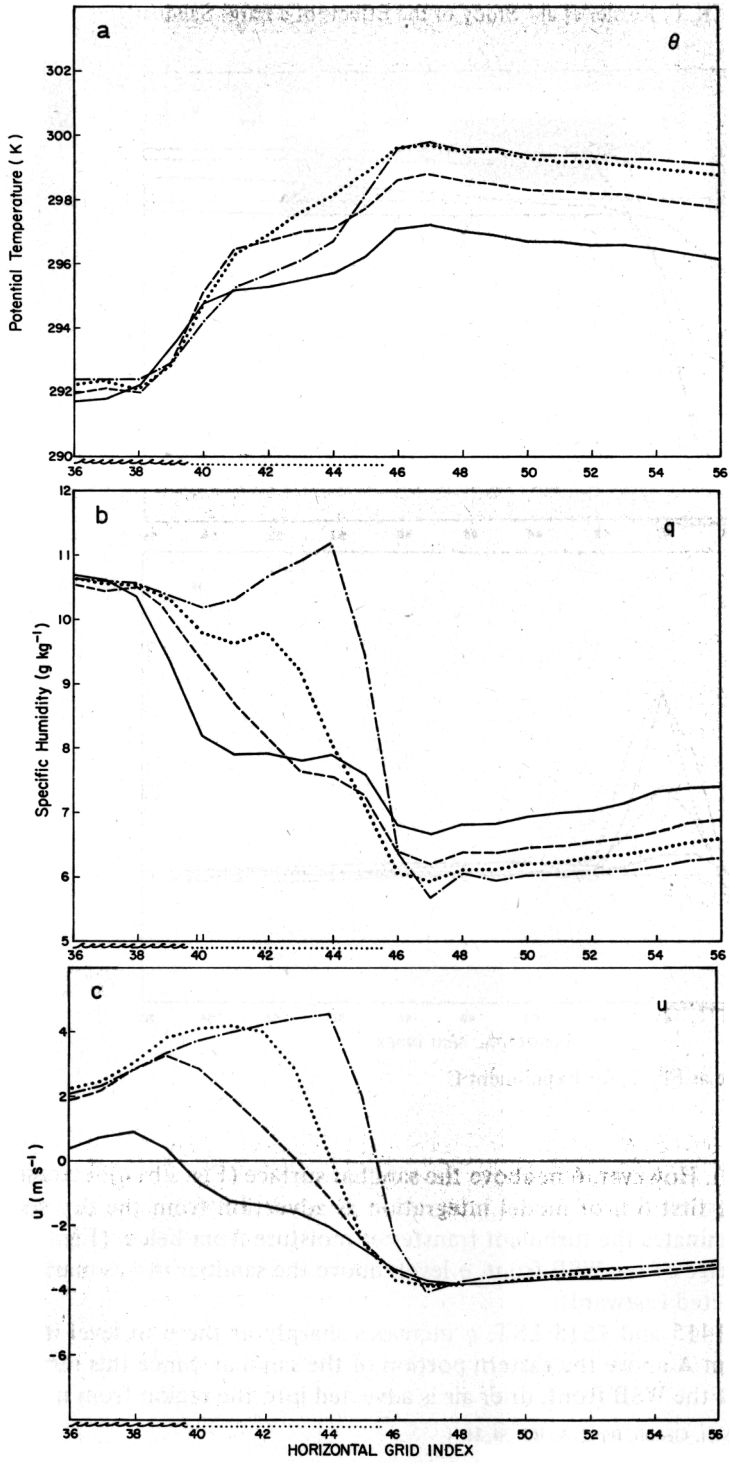
a
θ
Potential Temperature (K)
302
300
298
296
294
292
290
b
q
Specific Humidity (g kg⁻¹)
12
11
10
9
8
7
6
5
c
u
u (m s⁻¹)
4
2
0
-2
-4
-6
36
38
40
42
44
46
48
50
52
54
56
HORIZONTAL GRID INDEX

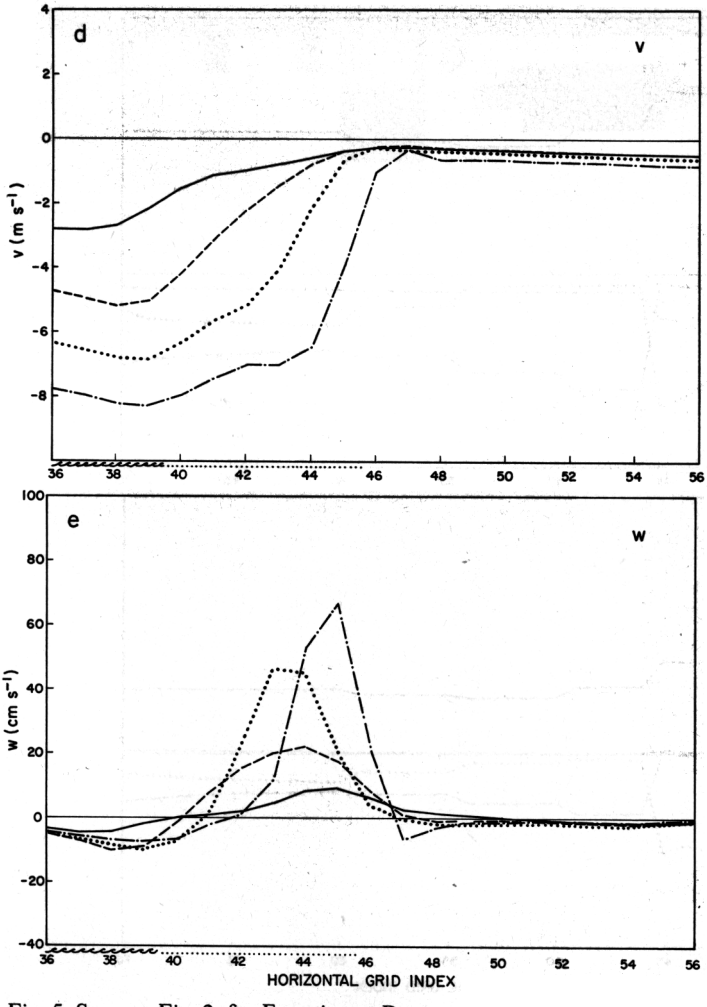

Fig. 5. Same as Fig. 2, for Experiment D

Thus, the increase in q must be ascribable to turbulent transfer. The region of slightly positive sensible heat flux at 1615 LST (Fig. 6) indicates that the surface layer has become stable east of the WSB front. Stabilization of the surface layer results in a sharp reduction of model-calculated turbulent exchange coefficients, but has a lesser effect immediately above the surface on the upward moisture flux from the sandbar. The net result is a convergence of the turbulent moisture flux at low levels east of the WSB front, similar to that reported by McCumber and Pielke [5] in their one-dimensional simulations.

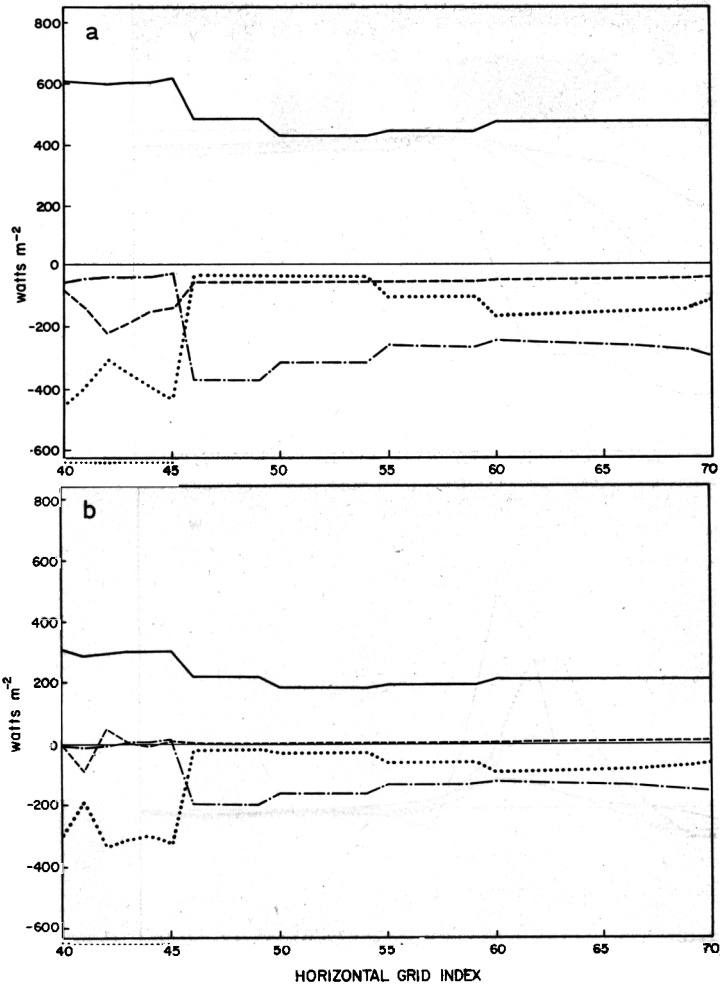

Fig. 6. Surface heat budget for Experiment A. a) 1215 LST and b) 1615 LST, where (——) net radiation; (— · — · —) sensible heat flux; (· · · · ·) latent heat flux; (- - - - -) soil heat flux. Units are W m^{-2}. Positive values are directed toward the ground surface

A similar q maximum is predicted above the east edge of the sandbar in Experiment D. Here the maximum lies to the west of the WSB front; at 1615 LST turbulent transfer from the surface adds moisture to the marine air advected inland by the WSB. In Experiment C, q decreases throughout the afternoon east of the WSB front, as the flux of moisture from the dry sand surface to the atmosphere is minimal, and the boundary layer continues

to deepen. The q increase after inundation in Experiment B results primarily from advection by the WSB; note the relationship between the u and q fields in Fig. 3.

9. Summary and Discussion

In this study we have attempted to simulate the effects of a large sandbar on sea-breeze development along the North Sea coast of the German state of Schleswig-Holstein. We have considered the effects of (1) land surface

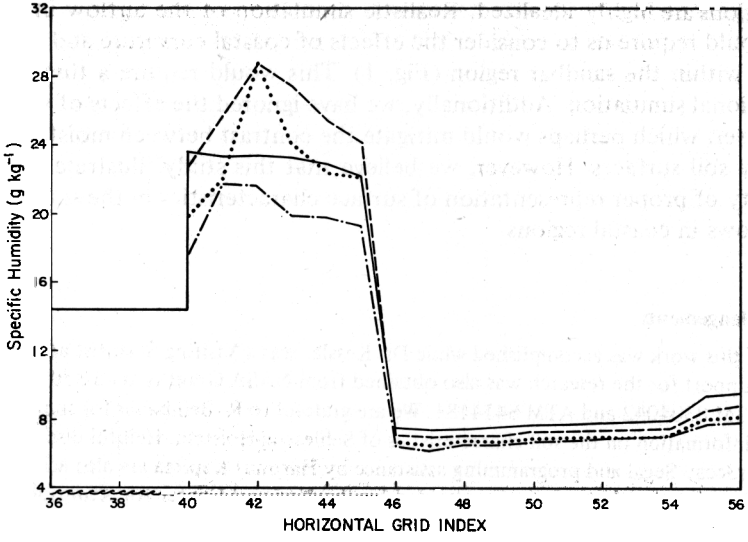

Fig. 7. Surface specific humidity (g/kg) for Experiment A. Legend as in Fig. 2

variability; (2) tidal inundation of the sandbar; and (3) inland penetration of an opposing sea breeze from the Baltic coast.

Our results indicate that a large sandbar can play a major role in sea breeze development. A sea breeze is a response to a local pressure gradient which results from differential heating of a surface. The presence of a moist sandbar adjacent to relatively dry soil adds an additional boundary across which differential heating can take place; this can act to diffuse the sea breeze front.

Tidal inundation of the sandbar removes this additional boundary. Thus the effect of inundation on a well-developed sea breeze involves both a translation and intensification of the sea breeze front.

Model results indicate that the Baltic sea breeze penetrates westward to the

North Sea sandbar under moderate easterly synoptic flow, eroding the horizontal temperature gradient above the sandbar-soil interface. In response, the west coast sea breeze is forced back toward the North Sea during the afternoon.

Low-level atmospheric humidity over the sandbar is governed primarily by advection when the model surface layer is unstable. Stabilization of the model surface layer results in turbulent moisture flux convergence above the sandbar, and a significant increase in low-level atmospheric humidities during the late afternoon.

Although we have based the initial and surface conditions for our simulations upon actual dry summer conditions in Schleswig-Holstein, these simulations are highly idealized. Realistic simulation of the airflow in this area would require us to consider the effects of coastal curvature and of the islands within the sandbar region (Fig. 1). This would require a three-dimensional simulation. Additionally, we have ignored the effects of vegetation cover, which perhaps would mitigate the contrast between moist sand and dry soil surfaces. However, we believe that this study illustrates the necessity of proper representation of surface characteristics in the simulation of airflows in coastal regions.

Acknowledgements

Much of this work was accomplished while Dr. Kessler was a Visiting Scientist at GKSS. Partial support for the research was also obtained from NASA Grant NAG 5-359 and NSF grants ATM 8304042 and ATM 8414181. We are grateful to R. Beinhauer for supplying us with information on the soil characteristics of Schleswig-Holstein. Helpful discussions with Mordecay Segal and programming assistance by Hartmut Kapitza are also acknowledged. Computational support was provided by the National Center for Atmospheric Research. NCAR is sponsored by the National Science Foundation.

We wish to thank Sara Rumley for her expert typing of the manuscript. The figures were prepared by Judy Sorbie.

References

1. Businger, J. A.: Turbulent Transfer in the Atmospheric Surface Layer. Workshop in Micrometeorology, Chapter 2. Amer. Met. Soc., Boston, Mass. (1973).
2. Deardorff, J. W.: Three-Dimensional Numerical Study of the Height and Mean Structure of a Heated Planetary Boundary Layer. Boundary-Layer Met. *1*, 81–106 (1974).
3. Mahrer, Y., Pielke, R. A.: A Numerical Study of the Air Flow over Irregular Terrain. Contrib. Atmos. Phys. *50*, 98–113 (1977).
4. Mahrer, Y., Pielke, R. A.: A Test of an Upstream Spline Interpolation Technique for the Advective Terms in a Numerical Mesoscale Model. Mon. Weath. Rev. *106*, 818–830 and 1758 (1978).

5. McCumber, M. C., Pielke, R. A.: Simulation of the Effects of Surface Fluxes of Heat and Moisture in a Mesoscale Numerical Model. Part 1: Soil Layer. J. Geophys. Res. *86*, 9929–9938 (1981).
6. O'Brien, J. J.: A Note on the Vertical Structure of the Eddy Exchange Coefficient in the Planetary Boundary Layer. J. Atmos. Sci. *27*, 1213–1215 (1970).
7. Ookouchi, Y., Segal, M., Kessler, R. C., Pielke, R. A.: Evaluation of Soil Moisture Effects on the Generation and Modification of Mesoscale Circulations. Mon. Weath. Rev. *112*, 2281–2292 (1984).
8. Paegle, J., Zdunkowski, W. G., Welch, R. M.: Implicit Differencing of Predictive Equations of the Boundary Layer. Mon. Weath. Rev. *104*, 1321–1324 (1976).
9. Pielke, R. A.: A Three-Dimensional Numerical Model of the Sea-Breezes over South Florida. Mon. Weath. Rev. *102*, 115–139 (1974).
10. Pielke, R. A., Mahrer, Y.: Technique to Represent the Heated-Planetary Boundary Layer in Mesoscale Models with Coarse Vertical Resolution. J. Atmos. Sci. *32*, 2288–2308 (1975).
11. Reineck, H. E.: Das Watt, Ablagerungs- und Lebensraum. Frankfurt: W. Kramer Verlag 1978.

Authors' addresses: R. C. Kessler, R. A. Pielke, J. McQueen, Department of Atmospheric Science, Colorado State University, Fort Collins, CO 80523, U.S.A.; D. Eppel, Institut für Physik, GKSS-Forschungszentrum, D-2054 Geesthacht, Federal Republic of Germany.

Appendix A. Soil Moisture Treatment

It is useful to begin by defining some characteristic soil parameters. The moisture content η is the volume of water (vapor plus liquid) contained in a unit volume of soil. It has units of $L^3 L^{-3}$.

The moisture potential ψ is the suction pressure required to extract water from the soil. ψ is conventionally given in units of length, symbolizing the height of a water column supportable by the required suction pressure (1 bar = 1000 cm). ψ is always negative; its absolute value decreases with increasing soil moisture.

The hydraulic conductivity (K_η) relates the soil moisture flux to the gradient of ψ. Only vertical gradients within the soil are considered in this study. Symbolically

$$w_s = K_\eta \rho_w \frac{\partial (\psi + z)}{\partial z} , \tag{A1}$$

where ψ_s is the soil moisture flux (positive downward) and ρ_w is the density of water. w_s has dimensions $M\ L^{-2}\ T^{-1}$; thus K_η has dimensions LT^{-1}. K_η increases as soil moisture content increases.

The diffusivity (D_η) is analogous to the exchange coefficient utilized in the representation of turbulent fluxes in the atmosphere. We define

$$D_\eta = K_\eta \frac{\partial \psi}{\partial \eta} . \tag{A2}$$

This allows (A1) to be written

$$w_s = D_\eta \rho_w \frac{\partial \eta}{\partial z} + K_\eta \rho_w \,. \tag{A3}$$

D_η has units $L^2 T^{-1}$.

ψ and K_η are functions of η and of soil type. The functional behavior of these variables is given by Clapp and Hornberger (1978):

$$\psi = \psi_s \left(\frac{\eta_s}{\eta}\right)^b \tag{A4}$$

$$K_\eta = K_{\eta_s} \left(\frac{\eta}{\eta_s}\right)^{2b+3} \,. \tag{A5}$$

Table A1. *Characteristic Soil Parameters*

Soil type	η_s ($cm^3 \cdot cm^{-3}$)	ψ_s (cm)	b	K_{η_s} (cm^2/sec)	C_i (cal/cm^3 K)
Clay loam	.476	−63.0	8.52	.000245	.293
Loam	.451	−47.8	5.39	.000695	.290
Loamy sand	.410	−9.0	4.38	.01563	.336
Sand	.395	−12.1	4.05	.0176	.350

Substituting (5) into (2) gives

$$D_\eta = -\frac{-bK_{\eta_s}\psi_s}{\eta}\left(\frac{\eta}{\eta_s}\right)^{b+3} \,. \tag{A6}$$

Subscript s refers to soil saturation. The saturation values of the parameters η, ψ, K_η, and D_η are inherent properties of the soil textural class, as is the exponent b in equations (A4), (A5), and (A6). η_s is frequently referred to as either the "field capacity" or the "porosity" of a soil.

In each grid column, continuity of moisture flux across the air-soil interface is required, i.e.,

$$w_a - (w_s)_G = 0 \,, \tag{A7}$$

where w_a is the turbulent flux of moisture at the surface, defined as

$$w_a = \rho u_* q_* \,. \tag{A8}$$

At the start of each time step, w_a is estimated from eq. (A8) and w_s from eq. (A1). If $(w_a - w_s)/w_a > 0.001$, an iterative process begins, whose steps are as follows:

(1) The equation

$$(w_s)_G^{u+1} = \delta (w_s)_G^u + (1-\delta) w_a; \quad 0 \leqslant \delta \leqslant 1 \tag{A9}$$

is used to force w_s toward w_a. The weighting factor δ is empirically chosen depending upon the relative humidity at the soil surface; McCumber and Pielke [5] indicate that δ must be skewed toward 1 for extremely dry soil surfaces in order to assure convergence.

(2) Eq. (A1) is inverted to obtain ψ at the air-soil interface from the new value of w_s.
(3) Eq. (A4) is inverted to obtain η at the air-soil interface from the new value of ψ_G.
(4) K_η and D_η are computed at the air-soil interface using eqs. (A5) and (A6), respectively.
(5) The convergence of ψ_G is checked, if ψ_G has not sufficiently converged, steps (2) through (4) are repeated.
(6) A surface relative humidity is computed from the equation

$$h = \exp - \left[\frac{g\psi_G}{R_v T_G} \right] \tag{A10}$$

The equations

$$q_G = hq_s \tag{A11}$$

$$q_s = 0.622 \frac{e_s}{p - 0.378\, e_s} \tag{A12}$$

$$e_s = 6.1078 \exp \left[17.269 \frac{T_G - 273.16}{T_G - 35.86} \right]$$

are then used to obtain the specific humidity at the surface, q_G.
(7) The new value of q_G is used to update w_a.
The sequence of steps (1) through (7) is repeated until w_a and w_s fulfill the convergence criterion. After w_a and w_s have converged, the prognostic equation for η

$$\rho_w \frac{\partial}{\partial t} \eta = \frac{\partial w_s}{\partial z} \tag{A14}$$

is solved. As a lower boundary condition on this equation, η is fixed at a specified depth in the soil. New values of K_η, ψ, and D, are then obtained from (A4), (A5), and (A6) using the updated values of η.
The soil volumetric heat capacity C and the thermal conductivity λ are functions of soil moisture. These parameters, required in the prognostic equation for θ_s, are obtained from the equations

$$C = (1 - \eta)\, C_i + \eta C_w$$

$$\begin{cases} \lambda = \exp\,[-(p_f + 2.7)]; & p_f \leqslant 5.1 \\ \lambda = 0.00041; & p_f > 5.1 \end{cases}$$

where p_f is the base 10 logarithm of the moisture potential ψ.
The surface albedo is a function of surface soil moisture and is obtained from

$$\begin{aligned} a_s &= 0.31 - 0.34\,\Delta; & \Delta &\leqslant 0.5 \\ a_s &= 0.14; & \Delta &> 0.5 \\ \Delta &= (\eta/\eta_s) \end{aligned} \tag{A17}$$

List of Symbols

a_s	soil albedo
b	dimensionless soil moisture exponent (function of soil textural class)
C	volumetric heat capacity

C_i	dry volumetric heat capacity for soil type i
C_w	volumetric heat capacity for water
e_s	saturation vapor pressure of air
g	gravitational constant
h	relative humidity of the surface soil
K_η	hydraulic conductivity
K_{η_S}	saturation hydraulic conductivity
L	latent heat of vaporization
p	atmospheric pressure
p_f	base 10 logarithm of the magnitude of the soil moisture potential
q	atmospheric specific humidity
q_G	soil surface specific humidity
q_s	saturation specific humidity
q_*	friction specific humidity
R_v	gas constant for water vapor
t	time
T_G	ground surface temperature
u, v, w	velocities
u_*	friction velocity
w_a	atmospheric surface moisture flux
w_s	soil moisture flux
$(w_s)_G$	surface soil moisture flux
η	soil volumetric moisture content
η_s	soil porosity
θ	potential temperature in the atmosphere
θ_s	potential temperature in the soil
θ_*	friction potential temperature
λ	soil thermal conductivity
ρ	air density
ρ_w	water density
ψ	soil moisture potential (as head of water, cm)

Printed in Austria